COMMUNICATION

Ionic Conduction Mechanism in High Concentration Lithium Ion Electrolytes

Received 00th January 20xx,
Accepted 00th January 20xx

DOI: 10.1039/x0xx00000x

Xiaobing Chen[a] and Daniel G. Kuroda[a]

The conduction mechanism of a family of high concentration lithium electrolytes (HCE) was investigated. It is found in all HCEs that the molecular motions are regulated by the anion size and correlated to the HCE ionic resistivity. From the results, a mechanism involving highly correlated ionic networks is derived.

Lithium ion batteries (LIB) have now become ubiquitous as an energy storage technology due to its rechargeability and comparatively large energy density. Hence, LIBs are now found in many devices ranging from portable electronics to, lately, electric vehicles.[1] While LIBs have many advantages over other battery chemistries, they still suffer from problems associated with electrochemical stability.[2, 3] Lately, a new generation of electrolytes based on highly concentrated salt solutions have been proposed to solve this problem.[4-8]

Highly concentrated electrolytes (HCE) consist of a lithium salt dissolved in an organic solvent at its limit of solubility (typically ~ 4M). At this concentration, the ratio of lithium ions to solvent molecules is 1:2 or lower. In the HCE, the lithium ions are not completely solvated by solvent molecules and rely on direct coordination to the anion to fulfil its tetrahedral solvation shell.[5, 9, 10] The extensive coordination of solvent molecules to the lithium centres confers special properties to the HCE, such as higher electrochemical stability.[4, 5] However, it is puzzling that the strong cation-anion interaction in the HCE does not completely inhibit the ionic transport, since HCEs have conductivities comparable to conventional electrolytes (i.e., 1 M or 1:9 molar ratio) even when their viscosity is typically an order of magnitude larger.[11, 12] The HCE comparatively large conductivity has been postulated to arise from a charge transport mechanism involving ion hopping.[11, 13]

Previous studies have delved into the structure and dynamics of HCEs to explain their high transport numbers.[10, 14-17] It has been proposed that HCEs present very fluid and extended ionic networks,[18] where lithium ions are in direct contact with both the solvent and the anions[5, 19, 20] and similar to an ionic liquid (IL).[21] Spectroscopic studies showed that most solvent molecules are coordinating to the lithium centers,[4, 22] while the small percentage of "free" solvent molecules corresponds to transient states created in picosecond time scale as a result of structural rearrangements in the ionic network.[10] Moreover, a similar picosecond time scale was derived for the ionic network rearrangements using neutron scattering.[17] While it is now clear that HCE ionic network rearrangements are ultrafast, the mechanism behind their high conductivity is still unclear.

Table 1. Anion chemical structure and viscosity (η) and conductivity (Ω) of the HCEs.

HCE	ACN/LiFSI	ACN/LiFTSI	ACN/LiTFSI	ACN/LiBETI
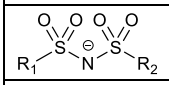	R1= -F R2= -F	R1= -F R2= $-CF_3$	R1= $-CF_3$ R2= $-CF_3$	R1= $-CF_2CF_3$ R2= $-CF_2CF_3$
Λ (mS/cm)	5.47 ± 0.04	3.34 ± 0.02	1.38 ± 0.04	0.44 ± 0.04
η (cP)	16.8 ± 0.5	63.1 ± 0.2	97.9 ± 0.2	316 ± 2

Here, a family of HCEs based on lithium sulfonylimide salts (Table 1) in acetonitrile-d3 (ACN) at a molar ratio of 1:2, was studied at both microscopic and macroscopic levels. At a macroscopic level, these HCEs present high ionic conductivities and viscosities (Table 1), as previously shown.[23] Interestingly, these HCEs also show decreasing conductivities as the anion size increases (from FSI to BETI), but their viscosity weighted conductivity (Walden product), as a crude representation of the number of charge carriers in the solution,[24] is comparable among all salts (within 40%, see Fig. S1, ESI) and hence, is not the reason behind the observed trend. While it is easy to conjecture that the changes in the macroscopic properties of these HCEs arise from the different chemical nature of the anion, ab-initio computations show that the four studied sulfonylimide anions share an analogous interaction potential with lithium ions (Fig. S2, ESI), which should result in a comparable number of charge carriers for these HCEs. Hence, it is clear that the ionic interaction picture in this family of high concentration sulfonylimide-based electrolytes is not sufficient to rationalize the observed conductivities in the HCE (Table 1), which opens a question of the molecular origins of these properties. To this end, the elementary molecular changes involved in the macroscopic properties of this HCE family were investigated using linear and time-resolved IR spectroscopies.

In this study, the nitrile (CN) stretch of ACN solvent molecules was used as a built-in molecular probe to study the changes in

[a] *Department of Chemistry, Louisiana State University, Baton Rouge, Louisiana 70803, United States*

[b] *Electronic Supplementary Information (ESI) available: Walden product, IR data, ab-initio potential and frequencies, and materials and methods. See DOI: 10.1039/x0xx00000x*

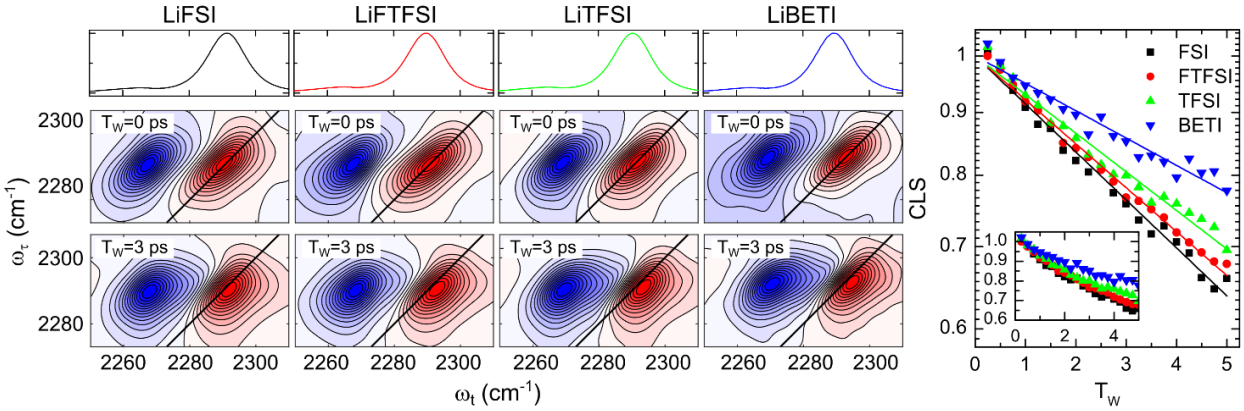

Fig. 1. FTIR and 2DIR spectra of HCE. Left panels show the FTIR (top row) and the 2DIR spectra at 0 ps (middle row) and 3 ps (bottom row) waiting times. Right panels contain normalized CLS of the studied HCEs and their corresponding modeling as described in the text. The right main panel has logarithmic scale while its inset has linear scale. Black squares, red circles, green up triangles, and blue down triangles correspond to HCEs containing LiFSI, LiFTFSI, LiTFSI, and LiBETI, respectively.

the molecular structure and interactions occurring in these HCEs. The CN stretch mode is particularly suitable because it reports the molecular environment motions sensed by individual ACN molecules, as previously shown.[25-30] The IR spectra of the four different electrolytes in the CN stretch region (Fig. 1) show a band around ~2290 cm^{-1} with a small shoulder located at ~2265 cm^{-1}, which have been assigned to the ACN nitrile stretch coordinated to Li+ and free, respectively.[25, 26] The large area ratio between the coordinated and free bands demonstrate that most solvent molecules are coordinated to the cations.[4, 12] The nitrile stretch bands have small frequency shifts (Fig. 1 and Table S2, ESI), but they become indistinguishable when they are centred (Fig. S3, ESI) evidencing a very similar environment sensed by the coordinated ACN molecules irrespective of the HCE anion identity.

The molecular picture derived from the linear IR spectra is in agreement with ab-initio molecular dynamic simulations (AIMD) of the HCEs. The AIMD radial distribution functions (RDF) show that four atoms, two from the solvent and two the anion, coordinate each lithium centre (Fig. 2) confirming the prevalence of ion-ion interactions in the investigated HCEs. Moreover, the AIMD reveals that every solvent molecule is within the first solvation shell of a lithium centre during the 200 ps trajectory, demonstrating that free solvent molecules are rare in these systems. The AIMDs also corroborate the direct interaction of anions with multiple lithium centres, or the so-called extended ionic network,[31, 32] in agreement with a previous study.[20] In addition, the AIMD reveals that a different number of anions are coordinated to each lithium centre. While the different coordination appears to contradict the presence of a single coordinated nitrile stretch band (~2285 cm^{-1} in Fig. 1), computations show that the probed CN stretches do not vary significantly for ion pairs with different anion identity and/or lithium coordination numbers (Table S3 and S4, ESI).

The dynamics of the molecular environment were derived from Two Dimensional IR (2DIR) spectroscopic studies. The 2DIR spectra in the nitrile stretch region for four HCEs at 0 ps (Fig. 1) show very similar spectral features among HCEs in direct correspondence to their FTIR. In general, all the investigated electrolytes have 2DIR spectra with one pair of peaks at the frequency of the coordinated CN stretch, which are originated from signals involving the υ=0 to υ=1 (red), and υ=1 to υ=2 (blue) vibrational states. Note that the 2DIR spectra do not show the peak corresponding to the free ACN molecules for any of the HCEs (Fig. S6, ESI) because of its small concentration and low transition dipole (Table S3, ESI).[25] Overall, the linear and non-linear IR spectra do not show any substantial difference in spectral features among HCEs, but the differences appear in the waiting time evolution (i.e., dynamics) of 2DIR spectra.

The time evolution of the 2DIR peaks (effect along different rows in Fig. 1) reveals a small but observable shape change from elongated along the diagonal line at 0 ps to slightly rounder and more upright 3 ps later due to the process of spectral diffusion. The spectral diffusion process represents at molecular level the thermal motions of the HCEs sensed by the coordinated ACN molecules.[33] The dynamics of the molecular environment, extracted using the CLS metric,[34] shows that all HCEs present dynamics in the picosecond time scale, but not sufficiently fast to achieve a total decorrelation within the 5 ps time window. A quantification of the CLS characteristic times using standard Kubo formalism (i.e., exponential decays)[35] reveals a decorrelation dynamics in the range of 10 to 20 ps for all HCEs, which is correlated with the anion size; i.e. larger anions have larger (slower) characteristic times.

The correlation between dynamics and the size of the anion as well as the picosecond characteristic time observed in the experiments suggest that fluctuations in the ion-ion interaction (i.e., reorganization of the ionic network) are the main mechanism behind the spectral diffusion process. In other words, bigger anions move slower leading to slower variation of the nitrile stretch frequencies of the coordinated ACN molecules. This hypothesis is supported by the AIMDs where it is observed not only that the molecular structure of the HCEs are dominated by ion-ion interactions (Fig. 2) but also that the HCE with the largest anion presents the longest ion pair lifetime ($\langle h(0)h(t)\rangle$ Fig. 2, Table 2 and ESI). Thus far, the results from experiments and theory suggest that thermal motions of the HCE ionic components are directly involved in the rearrangement of the ionic network, and consequently, are responsible for the spectral diffusion of the coordinated nitrile stretches observed in 2DIR spectra.

It has been previously hypothesized that in liquids dominated by ion-ion interactions, the making and breaking of ion pairs are the elementary steps preceding the molecular diffusion, and

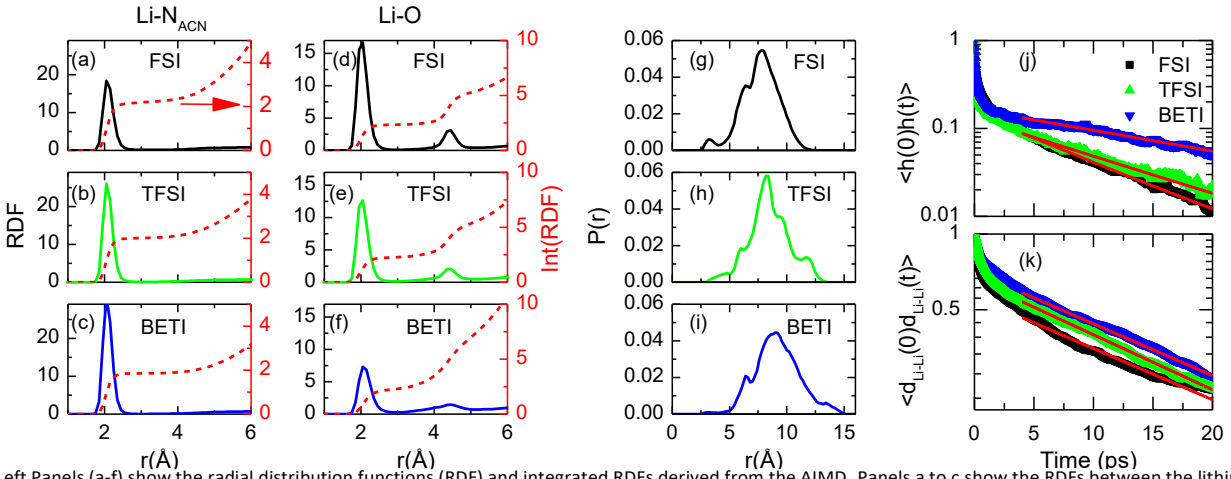

Fig. 2. Left Panels (a-f) show the radial distribution functions (RDF) and integrated RDFs derived from the AIMD. Panels a to c show the RDFs between the lithium ions and solvent nitrogen atoms, while panels d to f show the RDFs between the lithium ions and anion oxygen atoms. Red dashed lines and axis (right) correspond to the integrated RDFs. Middle panels (g-i) show the probability distributions for the distance between two lithium ions. Right panels (j and k) display the normalized correlation functions (ACFs) for ion pair and lithium-lithium distance, where the red lines represent their fittings as described in the text.

hence, the rate limiting steps that determine the viscosity.[36] Therefore, HCEs should follow the same governing laws given that ionic interactions control the elementary dynamics of these systems. Indeed, the spectral diffusion dynamics as a function of the macroscopic viscosity for the different HCEs (Fig. 3) shows a strong correlation (R^2=0.997), where the viscosity (Table 1) increases when the dynamics of the HCE is slower denoting that the elementary steps are also the making and breaking of the ion-ion interactions. In addition, the correlation between molecular motions and viscosity supports the idea that HCEs are analogues of ILs[37] and not ordinary ionic solutions.[21, 38]

A more interesting result observed here is the strong correlation (R^2=0.992) between ionic resistivity (reciprocal of ionic conductivity) and spectral diffusion dynamics (Fig. 3). As in the case of the viscosity, the direct relation between the molecular motions and the ionic resistivity points to the ionic network reorganization as the molecular origins of the resistivity. A similar relation between resistivity and molecular motions was observed in a deep eutectic solvent (DES) study and explained using a revolving-door mechanism.[39] Since the ACN-based HCEs are similar to an ionic DESs, it is possible that the same mechanism applies here and explain why the rate limiting step is related to charge transport. However, the study of an HCE family allows us to further infer the physical mechanism behind conductivity. The correlation between picosecond structural dynamics and resistivity implies that the ionic network reorganization is the molecular origin of resistivity for this family of HCEs. Unlike viscosity, the charge transport must involve a large degree of correlation among lithium sites experiencing changes in the coordination number. From a different perspective, if the structural correlation among lithium centres is not fulfilled, the limiting step in the HCE conductivity should be determined by the time needed to observe a "productive" charge transport steps, where all the involved ion pairs are dissociated simultaneously; rather than by the making and breaking of individual ion pairs.[40] In this last scenario, network rearrangement, sensed through spectral diffusion, will have a different time scale that will not correlate with resistivity. It is therefore concluded that the presence of a strong correlation among lithium motions must be part of the mechanism behind the low resistivity. These coordinated lithium motions should arise from the formation of a correlated ionic network that extends beyond the nanometer length scale and relates ultrafast local motions to larger length scale motions.

Table 2. Experimental and theoretical characteristic times.

HCE	⍰ (ps)		
	CLS	$\langle h(0)h(t)\rangle$	$\langle d_{Li-Li}(0)d_{Li-Li}(t)\rangle$
ACN/LiFSI	11.1 ± 0.3	7.9 ± 0.1	19.9 ± 0.1
ACN/LiFTFSI	12.2 ± 0.3	--	--
ACN/LiTFSI	13.8 ± 0.5	11.0 ± 0.1	21.1 ± 0.1
ACN/LiBETI	19.5 ± 0.9	17.2 ± 0.1	21.3 ± 0.1

Signatures of the correlated ionic network are derived from AIMDs through the time autocorrelation (ACF) and probability distributions of the distance between lithium pairs (d_{Li-Li}). The lithium-lithium distance ACF show a picosecond dynamics of ~ 20 ps, which is slower than that of the ion pair making and breaking ($\langle h(0)h(t)\rangle$ in Table 2). This difference in the dynamics of the two processes provides direct evidence of the strong correlation among lithium ions because the ion pair dynamics involves only near neighbours and the dynamics of the lithium-lithium distance contains all possible lithium pairs. In other words, if the different lithium centres have stochastic and uncorrelated motions beyond their first solvation shell, the dynamics of the lithium-lithium distance should have a much faster dynamics for the lithium pairs with the greatest separation and overall faster dynamics than that of ion pair lifetime. In fact, this is opposite to what is derived from the AIMD (Table 2). Furthermore, the probability distribution for the distance between two lithium ions (Fig. 2) also has the features of a strong correlated system as seen by its highly structured shape with a maximum at distances larger than 7 Å for all samples. The latter is an important aspect because it showcases that lithium ions in different solvation shell have high probability of remaining at a given distance (i.e., they remain correlated). However, it is also evident from the probability distributions that the correlation decreases by

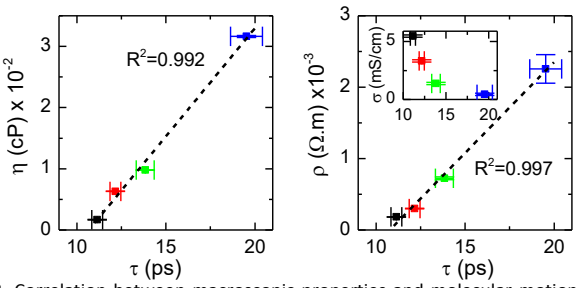

Fig. 3. Correlation between macroscopic properties and molecular motions for LiFSI/ACN (black), LiFTFSI/ACN (red), LiTFSI/ACN (green), and LiBETI/ACN (blue). Top panel has ionic resistivity and ionic conductivity as inset, while bottom panel displays viscosity. Black dashed lines represent the linear fittings of the data

becoming broader and less sharp as a function of the anion size (FSI>TFSI>BETI) in agreement with the increase in resistivity, lower conductivity, as observed for these HCEs (Table 1).

The observed correlation between cation in the HCE ionic network explains how HCEs transport charges efficiently by reorganizing simultaneously large regions of the ionic network, which produces charge transport but without physically moving ions throughout the system. This microscopic entanglement explains the surprisingly high ionic conductivity of the HCEs and its decrease as a function of the anion size. In fact, the extended correlated ionic network model is in good agreement with the lithium ion hopping mechanism previously proposed.[10, 13, 41]

In summary, this study demonstrates the presence of a strong correlation between the macroscopic properties and characteristic times of elementary thermal motions in ACN-sulfonylimide based HCEs. At a molecular level, the correlation highlights the defining role of the ion-ion interactions in forming a highly correlated ionic network and explains why they are the fundamental molecular limiting steps in these HCEs. In particular, a highly correlated ionic network is very important in defining the charge transport mechanism because it demonstrates that the HCE ionic conductivity occurs mainly throughout the rearrangement (making and breaking of ion pairs) of this network consisting of ions having long lasting correlated dynamics irrespective of the distance. These insights provide a physical mechanism for explaining the surprisingly high conductivity of HCEs and its dependence on the anion size.

The authors would like to thank the National Science Foundation (CHE-1751735) for financial support and LSU - High Performance Computing Center and the Louisiana Optical Network Initiative (LONI) for computer time.

Conflicts of interest

There are no conflicts to declare.

Notes and references

1. R. Korthauer, *Lithium-Ion Batteries: Basics and Applications*, Springer Berlin Heidelberg, 2018.
2. K. Liu, Y. Y. Liu, D. C. Lin, A. Pei and Y. Cui, *Sci. Adv.*, 2018, **4**.
3. Q. S. Wang, L. H. Jiang, Y. Yu and J. H. Sun, *Nano Energy*, 2019, **55**, 93-114.
4. J. Wang, Y. Yamada, K. Sodeyama, C. H. Chiang, Y. Tateyama and A. Yamada, *Nat. Commun*, 2016, **7**, 12032.
5. Y. Yamada, K. Furukawa, K. Sodeyama, K. Kikuchi, M. Yaegashi, Y. Tateyama and A. Yamada, *J. Am. Chem. Soc.*, 2014, **136**, 5039-5046.
6. K. Yoshida, M. Nakamura, Y. Kazue, N. Tachikawa, S. Tsuzuki, S. Seki, K. Dokko and M. Watanabe, *J. Am. Chem. Soc.*, 2011, **133**, 13121-13129.
7. T. Takashi, Y. Kazuki, H. Takeshi, T. Mizuho, N. Megumi, K. Yuichi, T. Naoki, D. Kaoru and W. Masayoshi, *Chem. Lett.*, 2010, **39**, 753-755.
8. V. Nilsson, R. Younesi, D. Brandell, K. Edstrom and P. Johansson, *J. Power Sources*, 2018, **384**, 334-341.
9. K. A. See, H.-L. Wu, K. C. Lau, M. Shin, L. Cheng, M. Balasubramanian, K. G. Gallagher, L. A. Curtiss and A. A. Gewirth, *ACS Appl. Mater. Interfaces*, 2016, **8**, 34360-34371.
10. S. R. G. Kankanamge and D. G. Kuroda, *J. Phys. Chem. B*, 2020, **124**, 1965-1977.
11. O. Borodin, J. Self, K. A. Persson, C. S. Wang and K. Xu, *Joule*, 2020, **4**, 69-100.
12. S. Sayah, A. Ghosh, M. Baazizi, R. Amine, M. Dahbi, Y. Amine, F. Ghamouss and K. Amine, *Nano Energy*, 2022, **98**.
13. K. Dokko, D. Watanabe, Y. Ugata, M. L. Thomas, S. Tsuzuki, W. Shinoda, K. Hashimoto, K. Ueno, Y. Umebayashi and M. Watanabe, *J. Phys. Chem. B*, 2018, **122**, 10736-10745.
14. L. M. Suo, Y. S. Hu, H. Li, M. Armand and L. Q. Chen, *Nat. Commun*, 2013, **4**, 1481.
15. J. T. Hu, Y. C. Ji, G. R. Zheng, W. Y. Huang, Y. Lin, L. Y. Yang and F. Pan, *Aggregate*, 2022, **3**.
16. S. Hwang, D. H. Kim, J. H. Shin, J. E. Jang, K. H. Ahn, C. Lee and H. Lee, *J. Phys. Chem. C*, 2018, **122**, 19438-19446.
17. F. Lundin, L. Aguilera, H. W. Hansen, S. Lages, A. Labrador, K. Niss, B. Frick and A. Matic, *Phys. Chem. Chem. Phys.*, 2021, **23**, 13819-13826.
18. J. Lim, K. Park, H. Lee, J. Kim, K. Kwak and M. Cho, *J. Am. Chem. Soc.*, 2018, **140**, 15661-15667.
19. R. Andersson, F. Aren, A. A. Franco and P. Johansson, *J. Electrochem. Soc.*, 2020, **167**.
20. K. Sodeyama, Y. Yamada, K. Aikawa, A. Yamada and Y. Tateyama, *J. Phys. Chem. C*, 2014, **118**, 14091-14097.
21. T. Mandai, K. Yoshida, K. Ueno, K. Dokko and M. Watanabe, *Phys. Chem. Chem. Phys.*, 2014, **16**, 8761-8772.
22. L. Wang, Z. Luo, H. Xu, N. Piao, Z. H. Chen, G. Y. Tian and X. M. He, *RSC Adv.*, 2019, **9**, 41837-41846.
23. S. D. Han, O. Borodin, D. M. Seo, Z. B. Zhou and W. A. Henderson, *J. Electrochem. Soc.*, 2014, **161**, A2042-A2053.
24. K. Kondo, M. Sano, A. Hiwara, T. Omi, M. Fujita, A. Kuwae, M. Iida, K. Mogi and H. Yokoyama, *J. Phys. Chem. B*, 2000, **104**, 5040-5044.
25. X. Chen and D. G. Kuroda, *J. Chem. Phys.*, 2020, **153**, 164502.
26. J. Barthel, R. Buchner and E. Wismeth, *J. Solution Chem.*, 2000, **29**, 937-954.
27. J.-S. Seo, B.-S. Cheong and H.-G. Cho, *Spectrochim. Acta, Part A*, 2002, **58**, 1747-1756.
28. P. Hilbig, L. Ibing, B. Streipert, R. Wagner, M. Winter and I. Cekic-Laskovic, *Curr. Top. Electrochem.*, 2018, **20**, 1-30.
29. B. Dereka, N. H. C. Lewis, Y. Zhang, N. T. Hahn, J. H. Keim, S. A. Snyder, E. J. Maginn and A. Tokmakoff, *J. Am. Chem. Soc.*, 2022, **144**, 8591-8604.
30. B. Dereka, N. H. C. Lewis, J. H. Keim, S. A. Snyder and A. Tokmakoff, *J. Phys. Chem. B*, 2021, DOI: 10.1021/acs.jpcb.1c09572.
31. M. McEldrew, Z. A. H. Goodwin, S. Bi, A. A. Kornyshev and M. Z. Bazant, *J. Electrochem. Soc.*, 2021, **168**.
32. J. H. Choi, H. Lee, H. R. Choi and M. Cho, *Annu. Rev. Phys. Chem.*, 2018, **69**, 125-149.
33. P. Hamm and M. Zanni, *Concepts and Methods of 2D Infrared Spectroscopy*, Cambridge University Press, Cambridge, 2011.
34. K. Kwak, D. E. Rosenfeld and M. D. Fayer, *J. Chem. Phys.*, 2008, **128**.
35. R. Kubo, *A stochastic theory of line shape*, John Wiley & Sons, 1969.
36. Z. Ren, A. S. Ivanova, D. Couchot-Vore and S. Garrett-Roe, *J. Phys. Chem. Lett.*, 2014, **5**, 1541-1546.
37. K. Ueno, K. Yoshida, M. Tsuchiya, N. Tachikawa, K. Dokko and M. Watanabe, *J. Phys. Chem. B*, 2012, **116**, 11323-11331.
38. D. J. Eyckens and L. C. Henderson, *Front. Chem.*, 2019, **7**.
39. D. Reuter, C. Binder, P. Lunkenheimer and A. Loidl, *Phys. Chem. Chem. Phys.*, 2019, **21**, 6801-6809.
40. S. R. G. Kankanamge, K. Li, K. D. Fulfer, P. Du, R. Jorn, R. Kumar and D. G. Kuroda, *J. Phys. Chem. C*, 2018, **122**, 25237-25246.
41. Y. Ugata, M. L. Thomas, T. Mandai, K. Ueno, K. Dokko and M. Watanabe, *Phys. Chem. Chem. Phys.*, 2019, **21**, 9759-9768.